Control Engineering Practice 59 (2017) 16–26

Contents lists available at ScienceDirect

Control Engineering Practice

journal homepage: www.elsevier.com/locate/conengprac

Robust pole location with experimental validation for three-phase grid-connected converters

Luiz A. Maccari Jr.[a,*], Humberto Pinheiro[b], Ricardo C.L.F. Oliveira[c], e Vinícius F. Montagner[b]

[a] Federal University of Santa Catarina, Blumenau, SC, Brazil
[b] Federal University of Santa Maria, Santa Maria, RS, Brazil
[c] University of Campinas, Campinas, SP, Brazil

ARTICLE INFO

Keywords:
Grid-connected converters
Robust control
Linear matrix inequalities
LCL filter
Pole location

ABSTRACT

This paper provides design and experimental validation of robust current controllers for three-phase grid-connected converters. The main objectives here are: (i) to show that a simple polytopic model can be used for designing robust controllers for predominately inductive grids; (ii) to help in the choice of the control design parameter, based on a trade-off between an upper bound of the transient settling times and the control gain sizes. Linear matrix inequality based conditions are used to design the robust control gains with lower numerical complexity than similar conditions on literature. It is shown that small values the radius of pole location lead to better bounds for the transient responses, at the price of higher control gains. Good tracking of references for the grid currents is also illustrated in practice, allowing the closed-loop system to inject active and reactive power into the grid. Simulation and experimental results prove that the system connected to the grid can provide three-phase currents complying with requirements of an important international standard.

1. Introduction

Grid-connected converters are of great importance in renewable energy source systems, as wind and photovoltaic power plants, playing the role of controlling active and reactive power (Liserre, Teodorescu, & Blaabjerg, 2006; Teodorescu, Liserre, & Rodríguez, 2011; Willis & Scott, 2000). In this context, the control of the grid injected current is fundamental, and standards as the IEEE 1547 present limits of distortion, as total harmonic distortion (THD) no larger than 5%, and prescribed limits of each harmonic for the grid injected current (see IEEE, 2011). For this application, LCL output filters can provide a compact structure efficient for harmonic attenuation. Such filters exhibit a resonance peak that needs to be damped and, to keep high efficiency, active damping becomes an interesting alternative. Among the grid current controllers, one can cite PI-based and resonant controllers (Castilla, Miret, Matas, Garcia de Vicuna, & Guerrero, 2009; Dannehl, Fuchs, Hansen, & Thøgersen, 2010; Eren, Bakhshai, & Jain, 2012; Khajehoddin, Karimi-Ghartemani, Jain, & Bakhshai, 2011, 2014; Maccari et al., 2012; Massing, Stefanello, Gründling, & Pinheiro, 2012; Parker, McGrath, & Holmes, 2014; Peña-Alzola et al., 2014; Zmood & Holmes, 2003). PI-based and resonant controllers place poles at limit of stability, reducing the stability margins. For continuous-time design, PI-based controllers convert the tracking of a sinusoidal reference in a regulation problem, placing poles near the origin, and resonant controllers place imaginary poles at chosen frequencies. Both techniques must cope with rejection of disturbances, as grid harmonic voltages, and operation under uncertain parameters. Aiming at set-point tracking, PI is insufficient or even incapable of dealing with disturbance rejection. The results in Sun, Li, and Lee (2016) demonstrate that, in PI design, the objectives of set-point tracking and disturbance rejection are sometimes conflictive. To improve the disturbance rejection, a two-degrees-of-freedom PI is analyzed. Moreover, an experimental application in Sun, Li, Hu, Lee, and Pan (2016) further shows that PI is quite weak in handling strong disturbances even when it was well tuned. A robust control solution that can well accommodate both the disturbances and uncertainties are necessary. In this sense, robust control techniques become of interest.

Robustness against disturbances and parametric uncertainties is a fundamental topic in control theory and applications (Ackermann, 1993; Sun, Li, & Lee, 2015; Zhou, Doyle, & Glover, 1996). In practical applications, as in grid-connected converters, one has that physical plant parameters are not precisely known, but lie inside intervals for which only the lower and upper bounds are given. This leads to the design of controllers that ensure stability and performance for the

* Corresponding author.
E-mail addresses: luizmaccari@gmail.com (L.A. Maccari), humberto.ctlab.ufsm.br@gmail.com (H. Pinheiro), ricfow@dt.fee.unicamp.br (R.C.L.F. Oliveira), vfmontagner@gmail.com (e.V.F. Montagner).

http://dx.doi.org/10.1016/j.conengprac.2016.10.013
Received 28 October 2015; Received in revised form 3 October 2016; Accepted 22 October 2016
Available online 30 November 2016

entire parameter space (e.g. robust $\mathcal{H}_2$, $\mathcal{H}_\infty$, DLQR, pole placement controllers). In order to obtain robust controllers given by a set of fixed gains, it is important to use suitable models for the plant, as for instance, polytopic or linear fractional models (Gahinet, Nemirovskii, Laub, & Chilali, 1995). It is also important to obtain control design conditions that are able to handle the model with uncertainties. In this sense, linear matrix inequality (LMI) based conditions are attractive. LMIs can easily include performance criteria, as $\mathcal{H}_2$ and $\mathcal{H}_\infty$ norms and pole placement, and are efficiently solved by specialized algorithms (Boyd, El Ghaoui, Feron, & Balakrishnan, 1994; Chilali, Gahinet, & Apkarian, 1999; Gahinet et al., 1995; Sturm, 1999). In case of plants affected by polytopic uncertainty, robust controllers can be designed in terms of a finite set of LMIs, assuring robust stability and performance for the whole domain of uncertainty. In this context, state feedback robust controllers are important, and the use of LMIs that provide less conservative results is of great interest, as given in de Oliveira, Bernussou, and Geromel (1999), Peaucelle, Arzelier, Bachelier, and Bernussou (2000), de Souza, Trofino, and de Oliveira (2000), Trofino and de Souza (2001), Shaked (2001), Apkarian, Tuan, and Bernussou (2001), de Oliveira, Geromel, and Bernussou (2002), Ebihara and Hagiwara (2004), Geromel and Korogui (2006), Oliveira, de Oliveira, and Peres (2011), and Morais, Braga, Oliveira, and Peres (2013). In general, the improvement of the accuracy of the synthesis conditions comes at the price of a larger computational effort. To establish a good tradeoff between complexity of the plant model and complexity of the control design conditions, aiming on robust stability and high performance, is still a matter that depends on the application under consideration.

The synthesis of state feedback robust controllers based on LMIs was successfully applied to power converters, with experimental validation. For instance, in Olalla, Leyva, El Aroudi, and Queinnec (2009, 2010, 2011), and Maccari, Montagner, Pinheiro, and Oliveira (2012), one has application of robust DLQR for DC–DC converters, with design in continuous-time domain. In Li, Sun, and Dai (2013), an $\mathcal{H}_\infty$ controller based on LMIs is designed to control the load voltage of an inductively coupled power transfer system. In Pereira, Flores, Bonan, Coutinho, and da Silva (2014), one has application of robust state feedback based on LMIs for uninterruptible power supplies (UPS), designed in continuous-time domain. Controllers designed in discrete-time domain are important for implementation in DSP and microcontrollers, suitable for industry applications. Discrete-time state feedback based design with experimental validation was addressed, for instance, in Ribas, Maccari, Pinheiro, Oliveira, and Montagner (2014), for $\mathcal{H}_\infty$ control of UPS output stage. In Gabe, Montagner, and Pinheiro (2009), one investigates a robust discrete-time control for grid-connected converters with experimental validation, using partial state feedback based on LMIs, with control gains design based on an iterative process, including resonant controllers. This work indicates the viability of this control design for this application. In Maccari et al. (2014), robust discrete-time pole location for single-phase grid-connected converters was addressed, with the design of the resonant controller gains not depending on iterative process. Robust stability and performance were illustrated, and the experimental validation of the results according to pertinent norm was carried out. In Maccari, Santini, Oliveira, and Montagner, (2013), a robust DLQR based on LMIs was successfully applied for three-phase grid-connected converters.

This work presents the design and analysis of a controller by means of LMIs for three-phase inverters connected to a grid subject to an uncertain inductance L_g. The contribution with respect to the robust pole location in Maccari et al. (2014) is its extension, with experimental validation, for the three-phase case, and also the analyses of the relationships between the radius r and the size of the control gains and with the settling times of the transient responses, the evaluation of phase and gain margins and the interpretation of the $\mathcal{H}_\infty$ norm as an output admittance of the closed-loop system. With respect to Maccari, Do Amaral Santini, Pinheiro, de Oliveira, and Foletto Montagner (2015), the advances are to provide a control design alternative based solely on the choice of one parameter, and to show that the numerical complexity of the control computation in this paper is lower than the one in Maccari et al. (2015), allowing a design much simpler and faster, mainly when the number of resonant controllers increase. Time domain simulations and experimental results confirm the good tracking of sinusoidal references in coordinates α and β, and also confirm the good quality of the grid injected three-phase currents, which comply with requirements of harmonic content from the IEEE 1547 Standard.

2. Continuous-time uncertain model

Consider the circuit depicted in Fig. 1. The LCL filter represents the plant, whose control variables are given by the output voltages of the three-phase inverter, the controlled outputs are the currents injected in the grid, and the disturbance inputs are given by the grid voltages, which can also include harmonics. The control signals are generated by a digital signal processor (DSP), based on the measurements of the state variables of the LCL filter. The grid is supposed as predominantly inductive, being modeled, per phase, by a voltage source in series with an inductance L_{g2}, assumed as an uncertain parameter, belonging to a given interval. It is known that the DC bus voltage control and the synchronization with the grid voltage are important issues for grid connected applications (Bianchi, Egea-Alvarez, Junyent-Ferré, & Gomis-Bellmunt, 2012; Umbrí et al., 2014). However, in the current paper it is assumed that the DC input voltage is constant and that the voltage at the point of common coupling (PCC) is already synchronized with the grid voltage (Cardoso, de Camargo, Pinheiro, & Gründling, 2008).

In order to obtain a model for the system described in Fig. 1, it is also assumed that the converter uses ideal switches and the switching frequency is much higher than the grid fundamental frequency, allowing, for control design purposes, to neglect the effect of PWM harmonics in the voltages generated by the converter (Teodorescu et al., 2011).

Thus a set of equations in the state variables for the LCL filter can be obtained, generating a model with 9 variables, 3 control inputs and 3 disturbance inputs, represented by

$$\frac{d\mathbf{x}_{abc}}{dt} = \mathbf{A}_{abc}\mathbf{x}_{abc} + \mathbf{B}_{uabc}\mathbf{u}_{abc} + \mathbf{B}_{dabc}\mathbf{v}_{dabc} \tag{1}$$

with

$$\mathbf{A}_{abc} = \begin{bmatrix} \mathbf{0}_{3\times3} & \mathbf{A}_{p1} & \mathbf{0}_{3\times3} \\ \mathbf{A}_{p2} & \mathbf{0}_{3\times3} & -\mathbf{A}_{p2} \\ \mathbf{0}_{3\times3} & \mathbf{A}_{p3} & \mathbf{0}_{3\times3} \end{bmatrix},$$

$$\mathbf{B}_{uabc} = \begin{bmatrix} -\mathbf{A}_{p1} \\ \mathbf{0}_{3\times3} \\ \mathbf{0}_{3\times3} \end{bmatrix}, \quad \mathbf{B}_{dabc} = \begin{bmatrix} \mathbf{0}_{3\times3} \\ \mathbf{0}_{3\times3} \\ -\mathbf{A}_{p3} \end{bmatrix} \tag{2}$$

and with

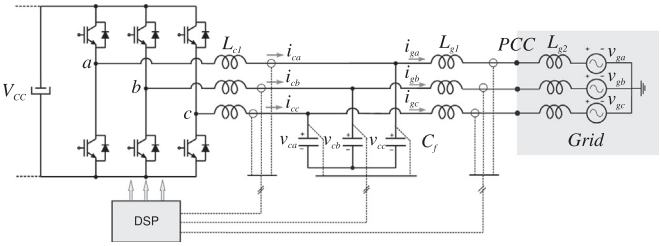

Fig. 1. Three-phase inverter connected to the grid by means of LCL filter.

$$\mathbf{A}_{p1}=\begin{bmatrix}-\frac{2}{3L_{c1}} & \frac{1}{3L_{c1}} & \frac{1}{3L_{c1}}\\ \frac{1}{3L_{c1}} & -\frac{2}{3L_{c1}} & \frac{1}{3L_{c1}}\\ \frac{1}{3L_{c1}} & \frac{1}{3L_{c1}} & -\frac{2}{3L_{c1}}\end{bmatrix},$$

$$\mathbf{A}_{p2}=\begin{bmatrix}\frac{1}{C_f} & 0 & 0\\ 0 & \frac{1}{C_f} & 0\\ 0 & 0 & \frac{1}{C_f}\end{bmatrix},$$

$$\mathbf{A}_{p3}=\begin{bmatrix}\frac{2}{3L_g} & -\frac{1}{3L_g} & -\frac{1}{3L_g}\\ -\frac{1}{3L_g} & \frac{2}{3L_g} & -\frac{1}{3L_g}\\ -\frac{1}{3L_g} & -\frac{1}{3L_g} & \frac{2}{3L_g}\end{bmatrix} \tag{3}$$

where

$$L_g = L_{g1} + L_{g2} \tag{4}$$

is also an uncertain parameter.

The state vector $\mathbf{x}_{abc}$, the input vector $\mathbf{u}_{abc}$ and the disturbances vector $\mathbf{v}_{dabc}$ are given as follows

$$\mathbf{x}_{abc}=\begin{bmatrix}i_{ca}\\ i_{cb}\\ i_{cc}\\ v_{ca}\\ v_{cb}\\ v_{cc}\\ i_{ga}\\ i_{gb}\\ i_{gc}\end{bmatrix},\quad \mathbf{u}_{abc}=\begin{bmatrix}u_a\\ u_b\\ u_c\end{bmatrix},\quad \mathbf{v}_{dabc}=\begin{bmatrix}v_{ga}\\ v_{gb}\\ v_{gc}\end{bmatrix} \tag{5}$$

To avoid the problem of coupling between phases, the three-phase system can be reduced to a decoupled two-phase system by means of the well known transformation of abc coordinates to $\alpha\beta0$ coordinates, whose transformation matrix is given by (Duesterhoeft, Schulz, & Clarke, 1951)

$$\mathbf{T}_{\alpha\beta0}=\frac{2}{3}\begin{bmatrix}1 & -\frac{1}{2} & -\frac{1}{2}\\ 0 & \frac{\sqrt{3}}{2} & -\frac{\sqrt{3}}{2}\\ \frac{1}{2} & \frac{1}{2} & \frac{1}{2}\end{bmatrix} \tag{6}$$

The change of coordinates is addressed by the multiplication of the vectors $\mathbf{u}_{abc}$ and $\mathbf{v}_{dabc}$ by the matrix $\mathbf{T}_{\alpha\beta0}$ and by the multiplication of the vector $\mathbf{x}_{abc}$ by the matrix

$$\mathbf{T}_a=\begin{bmatrix}\mathbf{T}_{\alpha\beta0} & \mathbf{0}_{3\times3} & \mathbf{0}_{3\times3}\\ \mathbf{0}_{3\times3} & \mathbf{T}_{\alpha\beta0} & \mathbf{0}_{3\times3}\\ \mathbf{0}_{3\times3} & \mathbf{0}_{3\times3} & \mathbf{T}_{\alpha\beta0}\end{bmatrix} \tag{7}$$

Then, the vectors in $\alpha\beta0$ coordinates are given by

$$\begin{aligned}\mathbf{x}_{\alpha\beta0}&=\mathbf{T}_a\mathbf{x}_{abc}\\ \mathbf{u}_{\alpha\beta0}&=\mathbf{T}_{\alpha\beta0}\mathbf{u}_{abc}\\ \mathbf{v}_{d\alpha\beta0}&=\mathbf{T}_{\alpha\beta0}\mathbf{v}_{dabc}\end{aligned} \tag{8}$$

Using the same reasoning, the system matrices in $\alpha\beta0$ coordinates can be written as

$$\begin{aligned}\mathbf{A}_{\alpha\beta0}&=\mathbf{T}_a^{-1}\mathbf{A}_{abc}\mathbf{T}_a\\ \mathbf{B}_{u\alpha\beta0}&=\mathbf{T}_a^{-1}\mathbf{B}_{uabc}\mathbf{T}_{\alpha\beta0}\\ \mathbf{B}_{d\alpha\beta0}&=\mathbf{T}_a^{-1}\mathbf{B}_{dabc}\mathbf{T}_{\alpha\beta0}\\ \mathbf{C}_{\alpha\beta0}&=\mathbf{C}_{abc}\mathbf{T}_a\end{aligned} \tag{9}$$

and the transformed system is described by

$$\begin{aligned}\dot{\mathbf{x}}_{\alpha\beta0}&=\mathbf{A}_{\alpha\beta0}\mathbf{x}_{\alpha\beta0}+\mathbf{B}_{u\alpha\beta0}\mathbf{u}_{\alpha\beta0}+\mathbf{B}_{d\alpha\beta0}\mathbf{v}_{d\alpha\beta0}\\ y_{\alpha\beta0}&=\mathbf{C}_{\alpha\beta0}\mathbf{x}_{\alpha\beta0}\end{aligned} \tag{10}$$

with the following state, control and disturbance vectors:

$$\begin{aligned}\mathbf{x}_{,\alpha\beta0}&=[i_{c\alpha}\ \ i_{c\beta}\ \ i_{c0}\ \ v_{c\alpha}\ \ v_{c\beta}\ \ v_{c0}\ \ i_{g\alpha}\ \ i_{g\beta}\ \ i_{g0}]\\ \mathbf{u}_{,\alpha\beta0}&=[u_\alpha\ \ u_\beta\ \ u_0]\\ \mathbf{v}_{,d\alpha\beta0}&=[v_{d\alpha}\ \ v_{d\beta}\ \ v_{d0}]\end{aligned} \tag{11}$$

Considering that the system is three wire, with no path to the current axis '0', the state space equations can be reorganized as follows (Duesterhoeft et al., 1951; Teodorescu et al., 2011)

$$\begin{bmatrix}\dot{\mathbf{x}}_\alpha\\ \dot{\mathbf{x}}_\beta\end{bmatrix}=\begin{bmatrix}\mathbf{A}(L_g) & \mathbf{0}\\ \mathbf{0} & \mathbf{A}(L_g)\end{bmatrix}\begin{bmatrix}\mathbf{x}_\alpha\\ \mathbf{x}_\beta\end{bmatrix}+\begin{bmatrix}\mathbf{B}_u & \mathbf{0}\\ \mathbf{0} & \mathbf{B}_u\end{bmatrix}\begin{bmatrix}u_\alpha\\ u_\beta\end{bmatrix}+\begin{bmatrix}\mathbf{B}_d(L_g) & \mathbf{0}\\ \mathbf{0} & \mathbf{B}_d(L_g)\end{bmatrix}\begin{bmatrix}v_{d\alpha}\\ v_{d\beta}\end{bmatrix} \tag{12}$$

In (12), one has two decoupled systems, one in coordinate α and the other in coordinate β. For control gain design purposes, it is possible to use a reduced state space representation, for example, the one associated with coordinate α. The control gains for coordinate β will be the same. The control law in α and β will differ only in their reference signals.

Omitting the subscripts α and β to simplify notation, the parameter-dependent state space model for control design purpose can be given by

$$\dot{\mathbf{x}}=\mathbf{A}(L_g)\mathbf{x}+\mathbf{B}_u u+\mathbf{B}_d(L_g)v_d \tag{13}$$

where

$$\mathbf{A}(L_g)=\begin{bmatrix}0 & -\frac{1}{L_{c1}} & 0\\ \frac{1}{Cf} & 0 & -\frac{1}{Cf}\\ 0 & \frac{1}{L_g} & 0\end{bmatrix},\quad \mathbf{B}_u=\begin{bmatrix}\frac{1}{L_{c1}}\\ 0\\ 0\end{bmatrix},$$

$$\mathbf{B}_d(L_g)=\begin{bmatrix}0\\ 0\\ -\frac{1}{L_g}\end{bmatrix},\quad \mathbf{x}=\begin{bmatrix}i_c\\ v_c\\ i_g\end{bmatrix} \tag{14}$$

The equation of the output is given by

$$y=\mathbf{C}_c\mathbf{x},\quad \mathbf{C}_c=[0\ \ 0\ \ 1] \tag{15}$$

3. Discrete-time polytopic model

Aiming on the use of a digital control technique, one can apply a discretization procedure in system (13). First notice that this system can be described by a continuous-time two-vertex polytopic model (Boyd et al., 1994)

$$\dot{\mathbf{x}}=\mathcal{A}(\boldsymbol{p})\mathbf{x}+\mathcal{B}_u(\boldsymbol{p})u+\mathcal{B}_d(\boldsymbol{p})v_d \tag{16}$$

where

$$(\mathcal{A}, \mathcal{B}_u, \mathcal{B}_d)(\boldsymbol{p}) = \sum_{i=1}^{2} p_i(\mathcal{A}, \mathcal{B}_u, \mathcal{B}_d)_i, \sum_{i=1}^{2} p_i = 1, \quad p_i \geq 0, \ i = 1, 2 \tag{17}$$

The vertices in (17) are given by the discretization of the respective matrices in (14), for $L_g = L_{gmin}$ and $L_g = L_{gmax}$. For a sufficiently small T_s, the continuous-time polytopic system with two vertices, $(\mathcal{A}, \mathcal{B}_u, \mathcal{B}_d)_i$, i=1,2, can be approximated by a discrete-time polytopic system with two vertices, as shown in Appendix A. This model is simple and suitable for control design, as will be seen in Section 5 in this paper, and can be written as

$$\mathbf{x}(k+1) = \mathbf{G}(\boldsymbol{p})\mathbf{x}(k) + \mathbf{H}(\boldsymbol{p})u(k) + \mathbf{H}_d(\boldsymbol{p})v_d(k) \tag{18}$$

where

$$(\mathbf{G}, \mathbf{H}, \mathbf{H}_d)(\boldsymbol{p}) = \sum_{i=1}^{2} p_i(\boldsymbol{I} + \mathcal{A}_i T_s, \mathcal{B}_{ui} T_s, \mathcal{B}_{di} T_s) \sum_{i=1}^{2} p_i = 1, \quad p_i \geq 0, \ i = 1, 2 \tag{19}$$

Assuming that there is a delay of one sample for implementation of the control signal by means of a DSP, one can rewrite (18) as (Aström & Wittenmark, 1997)

$$\begin{bmatrix} \mathbf{x}(k+1) \\ \theta(k+1) \end{bmatrix} = \begin{bmatrix} \mathbf{G}(\boldsymbol{p}) & \mathbf{H}(\boldsymbol{p}) \\ \mathbf{0}_{1\times 3} & 0 \end{bmatrix} \begin{bmatrix} \mathbf{x}(k) \\ \theta(k) \end{bmatrix} + \begin{bmatrix} \mathbf{0}_{3\times 1} \\ 1 \end{bmatrix} u(k) + \begin{bmatrix} \mathbf{H}_d(\boldsymbol{p}) \\ 0 \end{bmatrix} v_d(k)$$
$$y(k) = [\mathbf{C}_c \ \ 0] \begin{bmatrix} \mathbf{x}(k) \\ \theta(k) \end{bmatrix} \tag{20}$$

Based on the internal model principle Francis and Wonham (1976), to ensure tracking of a sinusoidal reference and also to ensure rejection of sinusoidal harmonic disturbances, it is necessary to have in the open loop transfer function poles at $e^{\pm j w_i T_s}$, where T_s is the sampling period and w_i are the frequencies to be tracked or rejected. Resonant controllers can be used to ensure these properties (Zmood & Holmes, 2003). One of these resonant controllers, written in discrete-time state space equations, can be given by the realization

$$\boldsymbol{\xi}(k+1) = \mathbf{R}\boldsymbol{\xi}(k) + \mathbf{T}e(k) \tag{21}$$

where

$$\mathbf{R} = \begin{bmatrix} a & b \\ 1 & 0 \end{bmatrix}, \quad \mathbf{T} = \begin{bmatrix} c \\ 0 \end{bmatrix}$$

and where $e(k)$ is the tracking error, given by

$$e(k) = i_{ref}(k) - y(k) \tag{22}$$

Assuming the entire state vector $\boldsymbol{\xi}(k)$ as output for the controller (21), one has that the transfer matrix from e to $\boldsymbol{\xi}$ is given by

$$\boldsymbol{\xi}(z) = ((z\mathbf{I} - \mathbf{R})^{-1}\mathbf{T})e(z) = \begin{bmatrix} \frac{cz}{z^2 - az - b} \\ \frac{c}{z^2 - az - b} \end{bmatrix} \tag{23}$$

Notice that the eigenvalues of $\mathbf{R}$ are also the poles of the resonant controllers in (23), since there is no cancellation of zeros and poles. Given a suitable choice of a and b, one has ensured the assignment of the pair of poles of the resonant controllers at $e^{\pm j w_i T_s}$.

A set of resonant controllers at the frequencies of the fundamental (w_o), third, fifth and seventh harmonics ($3w_o$, $5w_o$, $7w_o$) can be written as in (21) with dynamic matrices $\mathbf{R}_1$, $\mathbf{R}_3$, $\mathbf{R}_5$ and $\mathbf{R}_7$, respectively, and with input vectors $\mathbf{T}_1$, $\mathbf{T}_3$, $\mathbf{T}_5$ and $\mathbf{T}_7$ respectively. These harmonics are common in the grid and were chosen to compose the resonant controller in order to ensure its good attenuation (Teodorescu et al., 2011). This leads to an augmented state space model which has the plant states, the delayed control and the internal states of the resonant controllers, described in detail by (24):

$$\begin{bmatrix} \mathbf{x}(k+1) \\ \theta(k+1) \\ \xi_1(k+1) \\ \xi_2(k+1) \\ \xi_3(k+1) \\ \xi_4(k+1) \\ \xi_5(k+1) \\ \xi_6(k+1) \\ \xi_7(k+1) \\ \xi_8(k+1) \end{bmatrix} = \begin{bmatrix} \mathbf{G}(\boldsymbol{p}) & \mathbf{H}(\boldsymbol{p}) & 0 & 0 & 0 & 0 & 0 & 0 & 0 & 0 \\ \mathbf{0}_{1\times 3} & 0 & 0 & 0 & 0 & 0 & 0 & 0 & 0 & 0 \\ -\mathbf{T}_{1(1,1)}\mathbf{C}_c & 0 & \mathbf{R}_{1(1,1)} & \mathbf{R}_{1(1,2)} & 0 & 0 & 0 & 0 & 0 & 0 \\ \mathbf{0}_{1\times 3} & 0 & 1 & 0 & 0 & 0 & 0 & 0 & 0 & 0 \\ -\mathbf{T}_{3(1,1)}\mathbf{C}_c & 0 & 0 & 0 & \mathbf{R}_{3(1,1)} & \mathbf{R}_{3(1,2)} & 0 & 0 & 0 & 0 \\ \mathbf{0}_{1\times 3} & 0 & 0 & 0 & 1 & 0 & 0 & 0 & 0 & 0 \\ -\mathbf{T}_{5(1,1)}\mathbf{C}_c & 0 & 0 & 0 & 0 & 0 & \mathbf{R}_{5(1,1)} & \mathbf{R}_{5(1,2)} & 0 & 0 \\ \mathbf{0}_{1\times 3} & 0 & 0 & 0 & 0 & 0 & 1 & 0 & 0 & 0 \\ -\mathbf{T}_{7(1,1)}\mathbf{C}_c & 0 & 0 & 0 & 0 & 0 & 0 & 0 & \mathbf{R}_{7(1,1)} & \mathbf{R}_{7(1,2)} \\ \mathbf{0}_{1\times 3} & 0 & 0 & 0 & 0 & 0 & 0 & 0 & 1 & 0 \end{bmatrix} \begin{bmatrix} \mathbf{x}(k) \\ \theta(k) \\ \xi_1(k) \\ \xi_2(k) \\ \xi_3(k) \\ \xi_4(k) \\ \xi_5(k) \\ \xi_6(k) \\ \xi_7(k) \\ \xi_8(k) \end{bmatrix}$$
$$+ \begin{bmatrix} \mathbf{0}_{3\times 1} \\ 1 \\ 0 \\ 0 \\ 0 \\ 0 \\ 0 \\ 0 \\ 0 \\ 0 \end{bmatrix} u(k) + \begin{bmatrix} \mathbf{H}_d(\boldsymbol{p}) \\ 0 \\ 0 \\ 0 \\ 0 \\ 0 \\ 0 \\ 0 \\ 0 \\ 0 \end{bmatrix} v_d(k) + \begin{bmatrix} \mathbf{0}_{3\times 1} \\ 0 \\ T_{1(1,1)} \\ 0 \\ T_{3(1,1)} \\ 0 \\ T_{5(1,1)} \\ 0 \\ T_{7(1,1)} \\ 0 \end{bmatrix} i_{ref}(k), \ y(k) = [\mathbf{C}_c \ 0 \ 0 \ 0 \ 0 \ 0 \ 0 \ 0 \ 0 \ 0] \begin{bmatrix} \mathbf{x}(k) \\ \theta(k) \\ \xi_1(k) \\ \xi_2(k) \\ \xi_3(k) \\ \xi_4(k) \\ \xi_5(k) \\ \xi_6(k) \\ \xi_7(k) \\ \xi_8(k) \end{bmatrix}$$

In a more compact form, one has that (24) can be represented by

$$\boldsymbol{\rho}(k+1) = \mathcal{H}(\boldsymbol{p})\boldsymbol{\rho}(k) + \mathcal{H}_u u(k) + \mathcal{H}_d(\boldsymbol{p})v_d(k) + \mathcal{H}_r i_{ref}(k) y(k) = \boldsymbol{C}\boldsymbol{\rho}(k) \tag{25}$$

where $\boldsymbol{\rho} \in R^{12}$, $u \in R$, $y \in R$, $\mathcal{H} \in R^{12\times 12}$, $\mathcal{H}_u \in R^{12\times 1}$, $\mathcal{H}_r \in R^{12\times 1}$, $\mathcal{H}_d \in R^{12\times 1}$ and $\boldsymbol{C} \in R^{1\times 12}$. This augmented model will be used to design the control gains in the next section.

4. Control design

The block diagram of the control implementation for the three-phase system is given in Fig. 3. The states of the LCL filter are measured, producing the vector x_{abc}, which is digitally converted to $x_{\boldsymbol{abc}}(k)$. This vector is transformed to $\alpha\beta$ coordinates in the $abc\backslash\alpha\beta$ block. The new state vectors x_α and x_β become the inputs of the controller block, together with the references in $\alpha\beta$ coordinates $i_{ref\alpha}$ and $i_{ref\beta}$. The controller block provides the control signals u_α and u_β. In the PWM block, these control signals in $\alpha\beta$ coordinates are converted to the signals that drive the switches of the inverter to generate the desired voltages at the input of LCL filter. In the PWM block, a space vector modulation is used (Ranganathan, 1997).

To design the control gains, suppose the state feedback control law

$$u(k) = \mathbf{K}\boldsymbol{\rho}(k) = [\boldsymbol{K}_x \ \ K_\theta \ \ \boldsymbol{K}_\xi] \begin{bmatrix} \boldsymbol{x} \\ \theta \\ \boldsymbol{\xi} \end{bmatrix} \tag{26}$$

implemented as in the block diagram shown in Fig. 2. Notice that the states of the plant, in coordinates α or β, are multiplied by the gain vector $\boldsymbol{K}_x$, the delayed control signal has gain K_θ, and the states from the resonant controllers are multiplied by the gain vector $\boldsymbol{K}_\xi$. The control signal is given by the sum of these actions. Theorem 1 allows to compute all these gain entries simultaneously, as in Maccari et al. (2014).

Theorem 1. *For a given scalar r, $0 < r \leq 1$, if there exist symmetric positive definite matrices $\mathcal{S}_j \in R^{12\times 12}$, j=1,2, and matrices $\mathcal{G} \in R^{12\times 12}$ and $\mathcal{R} \in R^{1\times 12}$ such that*

$$\begin{bmatrix} \mathcal{G} + \mathcal{G}' - \mathcal{S}_j & \mathcal{G}'\frac{\mathcal{H}_j}{r} + \mathcal{R}'\frac{\mathcal{H}_{uj}}{r} \\ \frac{\mathcal{H}_j}{r}\mathcal{G} + \frac{\mathcal{H}_{uj}}{r}\mathcal{R} & \mathcal{S}_\ell \end{bmatrix} > \mathbf{0}, \quad j = 1, 2, \ \ell = 1, 2 \tag{27}$$

then the state feedback gain

$$\boldsymbol{K} = \mathcal{R}\mathcal{G}^{-1} \tag{28}$$

ensures:

(i) *closed-loop robust stability even for arbitrary changes of L_g;*
(ii) *that the eigenvalues of $\mathcal{H}(\boldsymbol{p}) + \mathcal{H}_u\mathbf{K}$ belong to the circle with center at the origin and with radius r, inside the unit circle;*

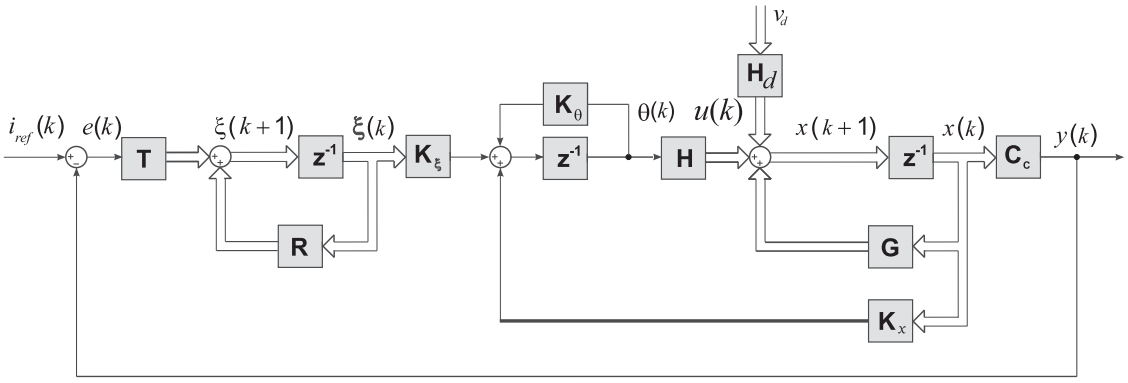

Fig. 2. Block diagram of the current controllers in α and in β coordinates.

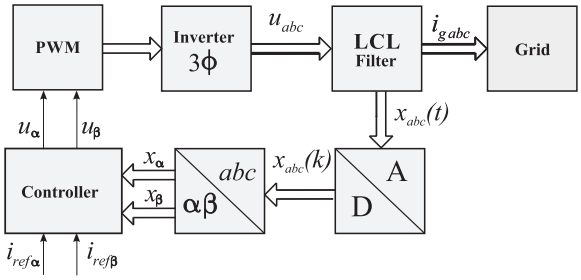

Fig. 3. Control scheme for the three-phase system.

Table 1
System parameters.

System description		
Nominal values	Power	5.4 kW
	Grid phase voltage	127 Vrms
	Grid phase current	14.14 Arms
	Grid frequency	60 Hz
	Switching frequency	10,020 Hz
	Sampling period	1/20 040 s
	V_{cc}	420 V
LCL filter	L_{c1}	1 mH
	L_{g1}	0.3 mH
	C_f	62 μF
Grid inductance	$L_{g2(min)}$	0 mH
	$L_{g2(max)}$	1 mH

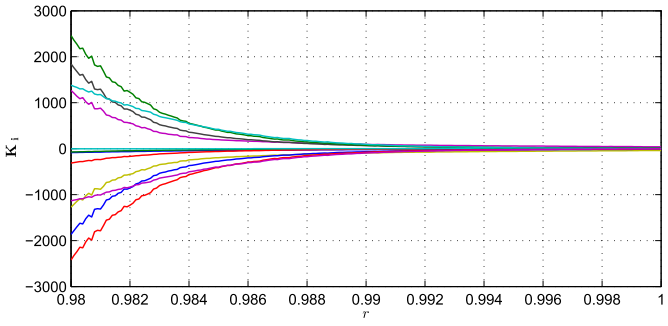

Fig. 4. Entries of the control gain vector as a function of the radius of the region for pole location.

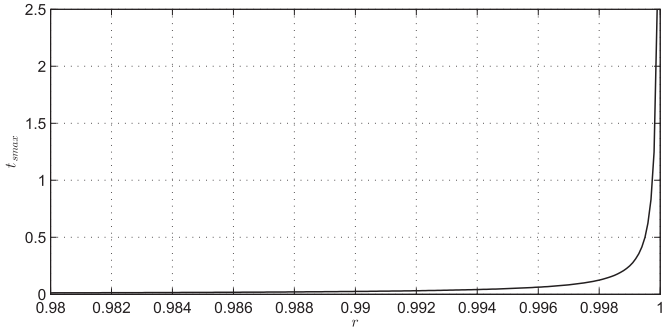

Fig. 5. Upper bound on the settling times of the transient responses as a function of the radius of the region for pole location.

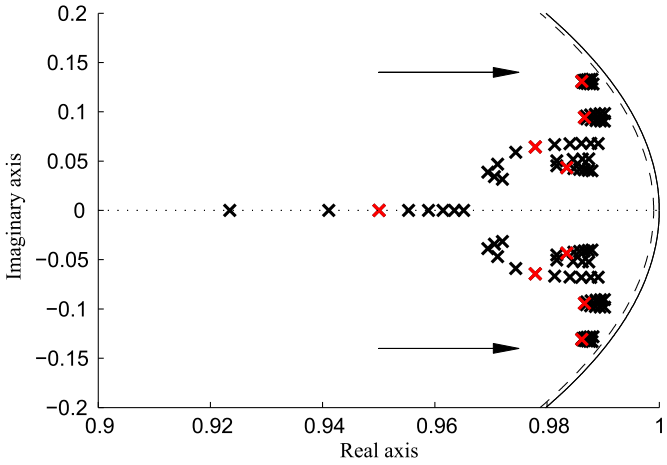

Fig. 6. Closed-loop poles for Lg from 0.3 mH to 1.3 mH. Circle with radius r=0.999 depicted with dashed line.

(iii) *the tracking of sinusoidal grid current references and rejection of grid voltage disturbances at frequencies of interest.*

The proof comes from Daafouz and Bernussou (2001).

In the next section, several analyses are carried out. For measures of reference tracking of the closed-loop system, the model

$$\boldsymbol{\rho}(k+1) = (\mathcal{H}(\boldsymbol{p}) + \mathcal{H}_u\boldsymbol{K})\boldsymbol{\rho}(k) + \mathcal{H}_r i_{ref}(k) y(k) = \boldsymbol{C}\boldsymbol{\rho}(k) \tag{29}$$

is used.

To verify the system capacity of rejecting harmonic disturbances, one uses

$$\boldsymbol{\rho}(k+1) = (\mathcal{H}(\boldsymbol{p}) + \mathcal{H}_u\boldsymbol{K})\boldsymbol{\rho}(k) + \mathcal{H}_d(\boldsymbol{p}) v_d(k) \qquad y(k) = \boldsymbol{C}\boldsymbol{\rho}(k) \tag{30}$$

For the measures of the phase and gain margin, the model

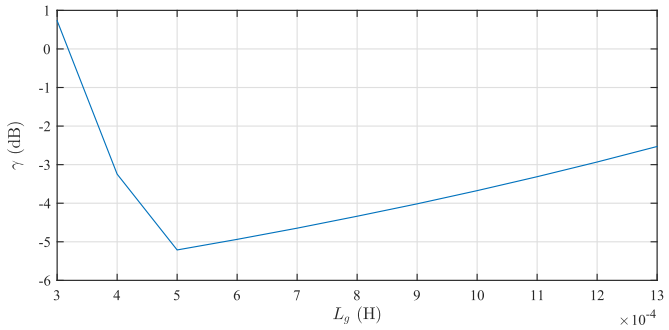

Fig. 7. $\mathcal{H}_\infty$ norm of the closed-loop system for values of L_g from 0.3 mH to 1.3 mH.

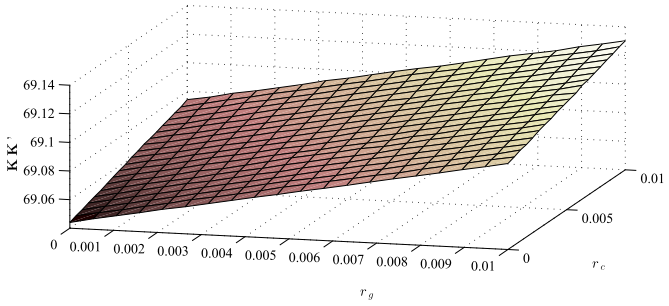

Fig. 8. Norm of the gain vector as a function of the parasitic resistances r_c and r_g of the filter.

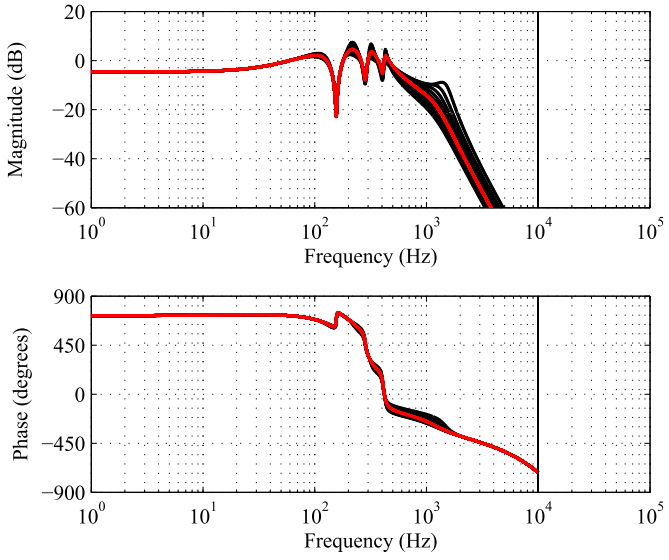

Fig. 9. Frequency responses of system with input i_{ref} and output i_g, given by model (30), for values of L_g in the interval of uncertainty.

$$\boldsymbol{\rho}(k+1) = (\mathcal{H}(\boldsymbol{p}) + \mathcal{H}_u\boldsymbol{K} + \mathcal{H}_r\boldsymbol{C})\boldsymbol{\rho}(k) + \mathcal{H}_r e(k) \qquad y(k) = \boldsymbol{C}\boldsymbol{\rho}(k) \tag{31}$$

is used.

5. Simulation results

The parameters in Table 1, borrowed from Maccari Jr. et al. (2013), are used here for control design and analyses. Notice that the uncertain parameter L_g belongs to [0.3, 1.3] mH.

Using Theorem 1 and the parameters in Table 1, one can find relations between the radius for pole location, r, with the size of the gain entries and also with the upper bound for the settling times of the transient responses. From Figs. 4 and 5, one can see, respectively, that

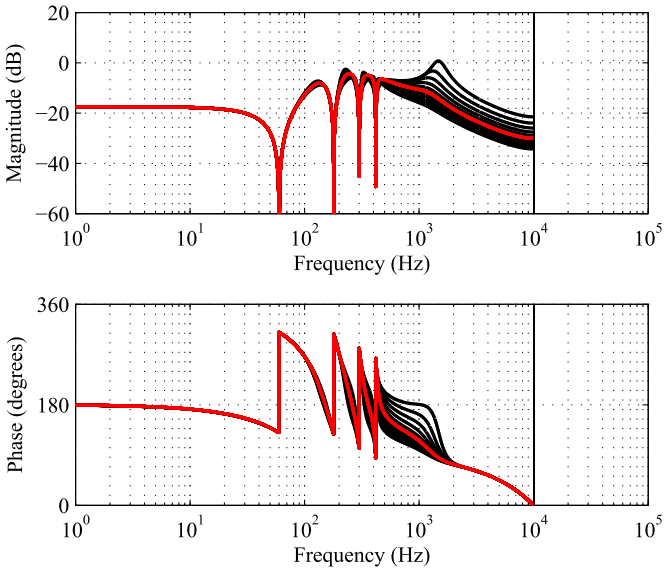

Fig. 10. Frequency responses of system with input v_d and output i_g, given by model (31), for values of L_g in the interval of uncertainty.

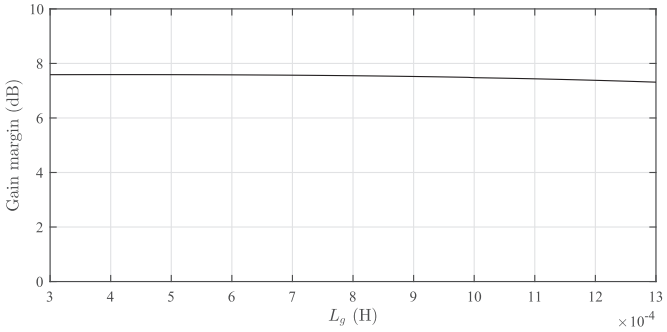

Fig. 11. Gain margin as a function of L_g.

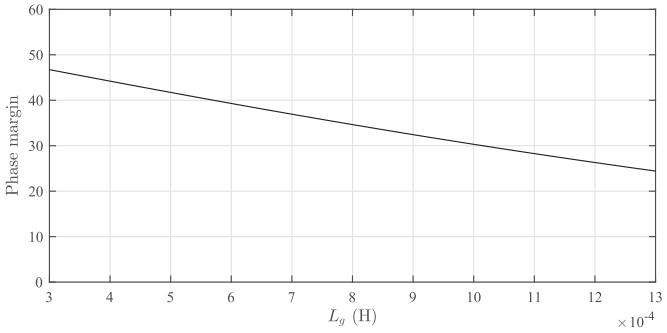

Fig. 12. Phase margin as a function of L_g.

with the increase of r, Theorem 1 provides controllers whose size of the control gain entries decrease. On the other hand, with the increase of r, the upper bound on the settling times of the transient responses also increase. This upper bound is given by

$$t_s = \frac{5T_s}{|\ln r|} \tag{32}$$

since for a pole $z=re^{j\,\theta}$ located at the border of the circle of radius r, centered at the origin of the complex plane, the mapping $e^{(\sigma+j\,\omega)T_s=z}$ leads to (32) for the expression of the settling time, under the criterium of 1% of error.

Using these informations, a suitable trade-off between the size of

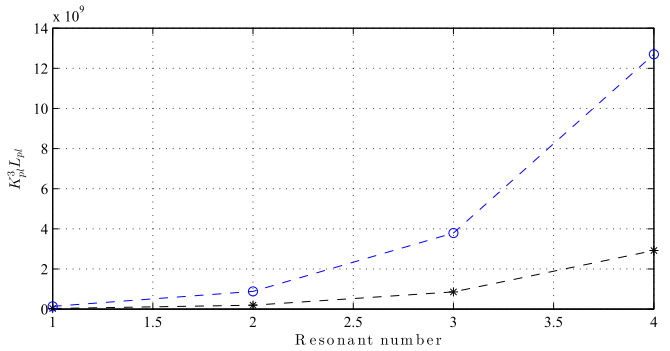

Fig. 13. Comparison of numerical complexity as a function of the number of resonant controllers n for the robust pole location controller (Theorem 1 – lower curve) and of the robust DLQR in Maccari et al. (2015), for DLQR controller (upper curve).

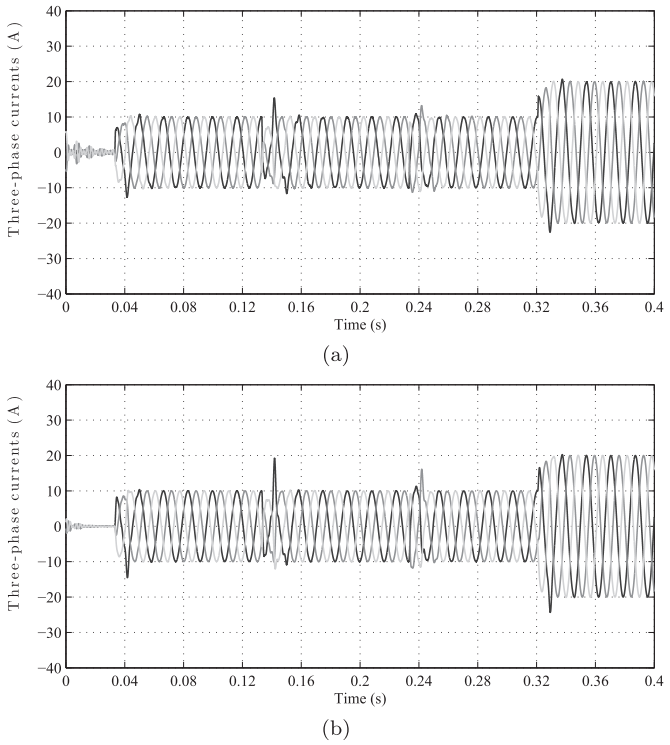

Fig. 14. (a) Simulation results: three-phase currents for $L_g = 0.3$ mH. (b) Simulation results: three-phase currents for $L_g = 1.3$ mH.

the control gain entries and the upper bound on the settling time of the transient responses can be investigated. For instance, in the case studied here, one has that r=0.999 provides control gains with small size and transient responses with settling times below the region of higher derivatives in curve shown in Fig. 5. With the choice of r=0.999, Theorem 1 provides the gains

$$\mathbf{K}' = \begin{bmatrix} -9.353075036915513 \\ -1.589585745204232 \\ -0.015790316776304 \\ -0.433936126512861 \\ 44.812204435984313 \\ -44.223640162858715 \\ 15.748275880415520 \\ -15.389082664601631 \\ 9.140650149699212 \\ -9.334723604102550 \\ 5.046556605805137 \\ -5.662179885219786 \end{bmatrix} \tag{33}$$

The gains (33) are expressed with a precision suitable for implementation in a floating point digital signal processor, as reported in Section 6. However, in the case of implementation in digital platforms with less precision, these gains can be represented with five digits, with no significant changes in the results. The closed-loop poles for the gains (33) are depicted in Fig. 6. These poles are located inside the circle with radius r=0.999, indicating stability for uncertain and time-invariant L_g. Moreover, the stability for variations on time of L_g are also ensured by the existence of the Lyapunov function

$$v = \boldsymbol{\rho}'(k)\left(\sum_{j=1}^{2} p_j \boldsymbol{S}_j\right)^{-1} \boldsymbol{\rho}(k), \quad \sum_{j=1}^{2} p_j = 1, \; p_j \geq 0 \tag{34}$$

with $\boldsymbol{S}_1$, $\boldsymbol{S}_2$ provided by the solution of Theorem 1.

Fig. 7 shows the $\mathcal{H}_\infty$ norm of the closed-loop system (30) for values of L_g from 0.3 mH to 1.3 mH. This norm can be seen as the peak of the Bode diagram of magnitudes (Boyd et al., 1994). Notice that the transfer function for (30) can be written as

$$G_{iv}(jw) = \frac{i_g(jw)}{v_d(jw)} \tag{35}$$

and that, for each value of L_g in the interval of uncertainty, the $\mathcal{H}_\infty$ norm can be seen as

$$\gamma = \max|G_{iv}(jw)| \tag{36}$$

Thus, the $\mathcal{H}_\infty$ norm can be interpreted for this application as the worst case admittance seen by the grid voltage. In this sense, lower values of γ mean better performance.

Another analysis that can be carried out is how the norm of the control gain vector is affected by parasitic resistances associated in series with the inductances of the filter. The resulting norms for the gains obtained from Theorem 1, with radius r=0.999, and with resistances r_c and r_g from 0 to 0.01 Ω are shown in Fig. 8. One can see that small parasitic resistances practically do not affect the norm of the control gain vector, confirming that this control design can be carried out, for instance, neglecting these parasitic resistances.

Results in the frequency domain are given, for L_g from 0.3 mH to

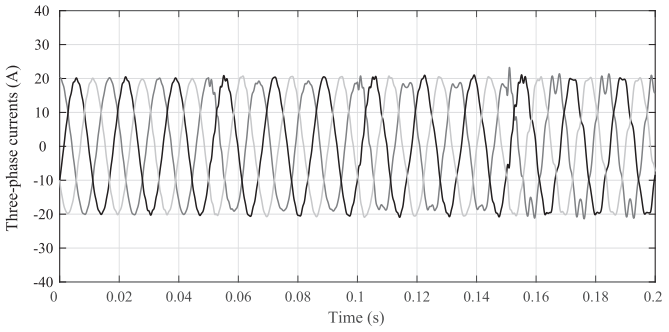

Fig. 15. Simulation results: three-phase currents injected to the grid in the presence of a grid voltage disturbance for the SRFPI controller.

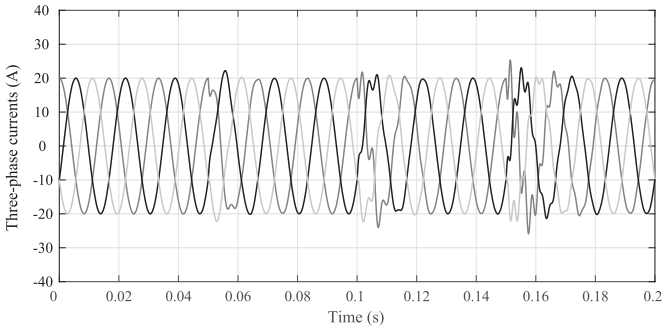

Fig. 16. Simulation results: three-phase currents injected to the grid in the presence of a grid voltage disturbance for the robust LMI controller.

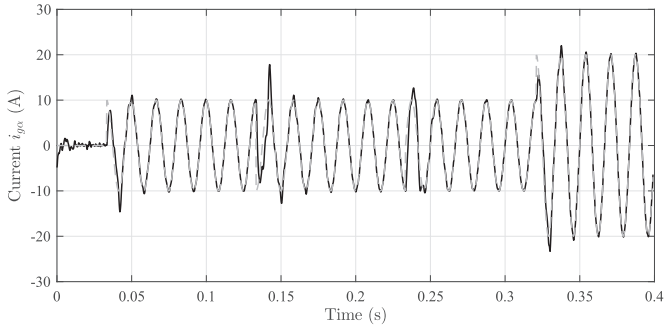

Fig. 17. Experimental results: currents i_g and i_{ref} (dashed) in coordinate α.

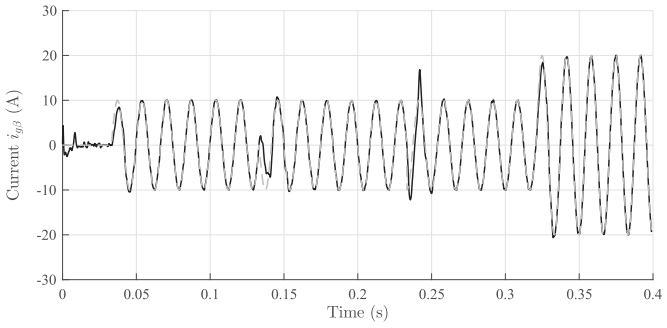

Fig. 19. Experimental results: currents i_g and i_{ref} (dashed) in coordinate β.

1.3 mH, to confirm the system capacity of tracking sinusoidal references and rejecting disturbances with harmonics. Fig. 9 shows that the gain at frequency 60 Hz is 0 dB and the phase is equivalent to 0°, ensuring tracking of sinusoidal reference with zero steady state error. Fig. 10 shows very small gains for the chosen odd harmonics, ensuring rejection of grid voltage disturbance at these frequencies.

The gain and phase margins, as functions of the grid inductance L_g are given, respectively, in Fig. 11 and in Fig. 12, obtained from the expression (25). These values of margins can be associated with closed-loop stability and suitable performances.

Notice that more resonant controllers as the ones in (21) can be used, to improve the rejection of disturbances, at the price of a design and an implementation of the control action with higher complexity. The numerical complexity of an LMI problem can be related to k^3L, k being the number of scalar variables and L the number of LMI rows (Gahinet et al., 1995). Thus, the numerical complexity associated to Theorem 1 will grow polynomially with the augment of the number of resonant controllers, as given in Fig. 13 (lower curve). For a comparison, the numerical complexity of the LMIs of a robust DLQR from Maccari et al. (2015) is also shown in Fig. 13 (upper curve). One can see clearly the advantages of the robust pole location given here, since its numerical complexity is always lower and also grows slowly than the one from the robust DLQR. Another advantage of this technique with respect to the robust DLQR is the simplicity of the design. Considering a general number of resonant controllers equal to n, in the robust pole location, the control designer only needs to choose one single parameter $0 < r \leq 1$, while in the robust DLQR, the control designer needs to choose $(4 + 2n) + 1$ parameters for the weighting matrices (assuming the weight matrix associated with the states as diagonal positive) and for the scalar of control weight in the cost function, being all of these design parameters positive and unbounded.

Three-phase time domain simulations are given in Fig. 14. The references for the sinusoidal currents are produced in α and in β coordinates, with changes of phase and amplitude. The simulation results in Fig. 14 illustrate fast transient recovers and the good steady state behaviors, being suitable for this application.

In order to have a comparison, a synchronous reference frame proportional-integral (SRFPI) controller is designed here. The SRFPI controller is implemented using an active damping strategy based on a virtual resistor, as described in Zhang, Dragicevic, Vasquez, and Guerrero (2014). The design assumes L_g=0.65 mH as nominal value of grid inductance. The controller gains K_p, K_i and the value of virtual resistor R_d are given by

$$K_p = 0.433K_i = 433R_d = 0.5 \tag{37}$$

Figs. 15 and 16 show, respectively, the results of the closed-loop system with the SRFPI and with the proposed robust LMI controller. The grid voltage, in one of the phases, is given by

$$220[\sin(2\pi 60t) + h(t-0.05)0.1\sin(2\pi 180t) + h(t-0.1)0.1\sin(2\pi 300t) + h(t-0.15)0.1\sin(2\pi 420t)] \tag{38}$$

where the function $h(t)$ is the Heaviside step function.

In Fig. 15, one can see that the SRFPI controller has a poor rejection of disturbance, mainly for higher frequency harmonics.

On the other hand, in Fig. 16, one can observe that, after the transient recovers, the harmonics from the grid are rejected by the robust LMI controller, leading to a much better performance. It is worth to mention that the tuning of the control gains for multiple SRFPIs becomes more difficult (Teodorescu et al., 2011). This problem does not occur with the proposed LMI based strategy because all the control gains here are obtained simultaneously, by means of the choice of one single design parameter.

6. Experimental results

To confirm the practical viability of the robust pole location controller for three-phase grid-connected applications, a prototype was used to obtain experimental results. The prototype is controlled by a DSP TMS320F28335 from Texas Instruments. The gains (33) were used in the DSP code. The LCL filters use Semikron inductors and Epcos capacitors. The sensors of voltage are based on transformers and the sensors of current are from LEM. The inverter is from Semikron, based on IGBTs. The system parameter values are given in Table 1. The experimental results presented in this section were obtained with the converter connected to the grid, whose impedance value is not

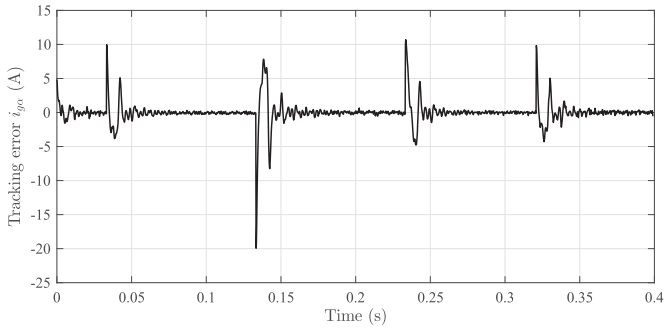

Fig. 18. Experimental results: tracking error from Fig. 17.

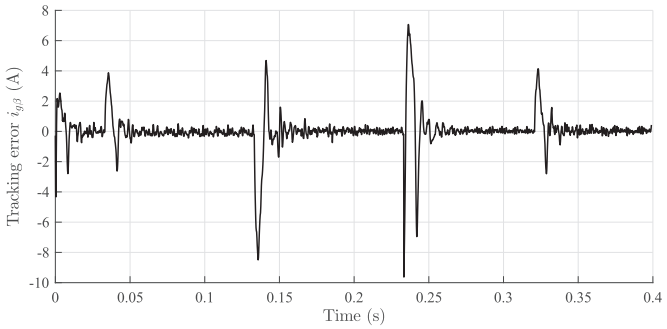

Fig. 20. Experimental results: tracking error from Fig. 19.

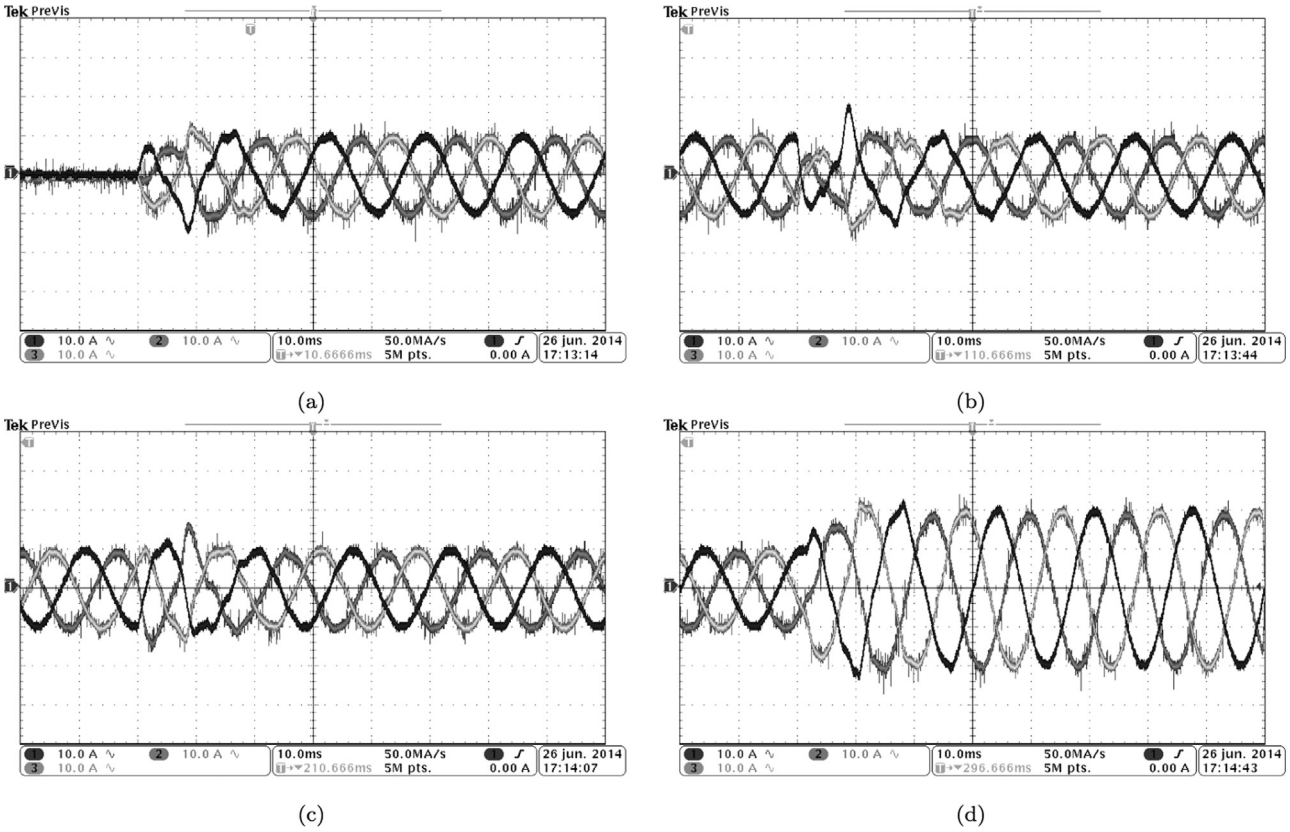

Fig. 21. Experimental results: (a) Response on start-up. (b) Response for a variation on the reference current phase of 180°. (c) Response for a variation on reference current phase of 90°. (d) Response for a variation on the reference current amplitude from 10 A to 20 A.

measured or identified in real time.

The experimental results for the grid current in coordinate α are given in Fig. 17, where the reference and the output are shown. One can see the good tracking for changes of phase and amplitude for the grid current. The tracking error is given in Fig. 18 and converges to zero after the transients.

The experimental results for the grid current in coordinate β are given in Fig. 19, where, again, one observes a good tracking of reference. As in the case of coordinate α, the tracking error in coordinate β, given in Fig. 20, converges to zero after each transient.

The grid injected currents in coordinates *abc* for the same variations of references given in Fig. 17 and in Fig. 19 are shown in Fig. 21. The situations shown in Fig. 21 represent the injection of reactive and active power into the grid. Notice that the experimental results, obtained with an uncertain grid impedance value, have good correspondence with the simulation results presented in Fig. 14. This corroborates that the plant model used here, with a third order system affected by one uncertain parameter, is suitable for control design for this application. Possible unmodeled dynamics and even nonlinearities in the real plant are handled by the feedback controller. Each one of the tests in Fig. 21 represents a detailed view of each transient caused by variations in the references in α and β coordinates. One can see the stable behavior, the fast transient recovers and the overall good quality of the waveforms of the closed-loop system.

A detailed view of the steady state currents injected in the grid is shown in Fig. 22. The analysis of harmonics according to IEEE Standard 1547 of the waveform i_{ga} in Fig. 22 leads to Fig. 23. One can see that the harmonics in this waveform comply with the bounds from IEEE Standard 1547, confirming the suitable performance of this robust controller for three-phase converters.

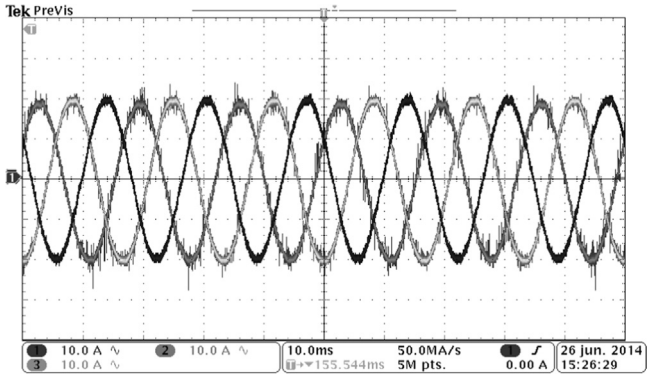

Fig. 22. Experimental results: steady state currents injected in the grid.

7. Conclusion

This work presented the design, analysis and experimental validation of a robust pole location controller for three-phase grid-connected converters. As one of the main points, one can cite that the model of the

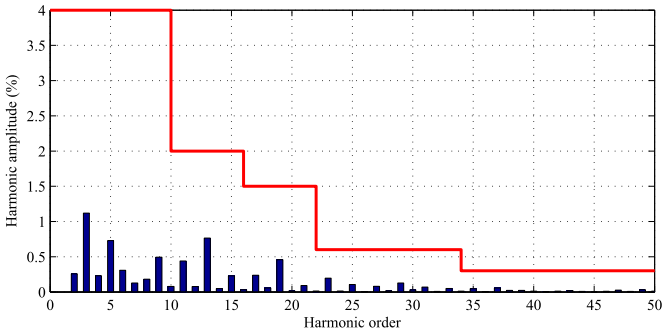

Fig. 23. Harmonic components for the waveform i_{ga} in Fig. 22.

grid based solely on an uncertain inductance, and the model of the LCL filter neglecting small parasitic resistances is sufficient to design control gains that allow to obtain simulation and experimental results of good quality, respecting the limits of harmonic content of an important international standard. It is shown that the $\mathcal{H}_\infty$ norm of the closed-loop system can be interpreted as the worst case admittance seen by the grid voltage. Comparisons with a similar technique, a robust DLQR, illustrate that the proposed controller has much lower numerical complexity and is easier to be designed. Comparison with a traditional PI based controller show the superiority of the proposed technique for harmonic rejection. Thus, this paper provides an interesting alternative for robust current control design and validation for three-phase grid-connected converters.

Acknowledgment

To the Brazilian agencies CNPq and CAPES.

Appendix A

The discretization with the zero-order hold method and sampling period T_s leads to Aström and Wittenmark (1997)

$$\mathbf{x}(k+1) = e^{\mathcal{A}(\boldsymbol{p})T_s}\mathbf{x}(k) + \int_0^{T_s} e^{\mathcal{A}(\boldsymbol{p})\tau}\mathcal{B}_u(\boldsymbol{p})d\tau\ u(k) + \int_0^{T_s} e^{\mathcal{A}(\boldsymbol{p})\tau}\mathcal{B}_d(\boldsymbol{p})d\tau\ v_d(k) \tag{39}$$

The expansion in power series of the exponential function on the first term of (39) results in

$$e^{\mathcal{A}(\boldsymbol{p})T_s} = \boldsymbol{I} + \mathcal{A}(\boldsymbol{p})T_s + \sum_{j=2}^{\infty}\frac{\mathcal{A}(\boldsymbol{p})^j T_s^j}{j!} \tag{40}$$

Assuming T_s is sufficiently small, one can neglect the terms

$$\sum_{j=2}^{\infty}\frac{\mathcal{A}(\boldsymbol{p})^j T_s^j}{j!} \tag{41}$$

and write

$$e^{\mathcal{A}(\boldsymbol{p})T_s} = \boldsymbol{I} + \mathcal{A}(\boldsymbol{p})T_s \tag{42}$$

From (39), one has that

$$\int_0^{T_s} e^{\mathcal{A}(\boldsymbol{p})\tau}\mathcal{B}_u(\boldsymbol{p})d\tau = \int_0^{T_s}\left(\boldsymbol{I} + \sum_{k=1}^{\infty}\frac{\mathcal{A}(\boldsymbol{p})^k\tau^k}{k!}\right)\mathcal{B}_u(\boldsymbol{p})d\tau \tag{43}$$

Again, for a sufficiently small T_s, (43) can be rewritten as

$$\mathcal{B}_u(\boldsymbol{p})T_s \tag{44}$$

Following the same reasoning, one has that the approximate discretization of the disturbance input vector is described by

$$\mathcal{B}_d(\boldsymbol{p})T_s \tag{45}$$

References

Ackermann, J. (1993). *Robust control: Systems with uncertain parameters* London, England: Springer Verlag.

Apkarian, P., Tuan, H. D., & Bernussou, J. (2001). Continuous-time analysis, eigenstructure assignment, and $\mathcal{H}_2$ synthesis with enhanced linear matrix inequalities (LMI) characterizations. *IEEE Transactions on Automatic Control*, 46, 1941–1946.

Aström, K., & Wittenmark, B. (1997). *Computer-controlled systems: Theory and design*. Prentice Hall.

Bianchi, F. D., Egea-Alvarez, A., Junyent-Ferré, A., & Gomis-Bellmunt, O. (2012). Optimal control of voltage source converters under power system faults. *Control Engineering Practice*, 20, 539–546.

Boyd, S., El Ghaoui, L., Feron, E., & Balakrishnan, V. (1994). *Linear matrix inequalities in system and control theory*. Philadelphia, PA: SIAM Studies in Applied Mathematics.

Cardoso, R., de Camargo, R. F., Pinheiro, H., & Gründling, H. A. (2008). Kalman filter based synchronisation methods. *IET Generation, Transmission Distribution*, 2, 542–555.

Castilla, M., Miret, J., Matas, J., Garcia de Vicuna, L., & Guerrero, J. M. (2009). Control design guidelines for single-phase grid-connected photovoltaic inverters with damped resonant harmonic compensators. *IEEE Transactions on Industrial Electronics*, 56, 4492–4501.

Chilali, M., Gahinet, P., & Apkarian, P. (1999). Robust pole placement in LMI regions. *IEEE Transactions on Automatic Control*, 44, 2257–2270.

Daafouz, J., & Bernussou, J. (2001). Parameter dependent Lyapunov functions for discrete time systems with time varying parameter uncertainties. *Systems & Control Letters*, 43, 355–359.

Dannehl, J., Fuchs, F., Hansen, S., & Thøgersen, P. (2010). Investigation of active damping approaches for PI-based current control of grid-connected pulse width modulation converters with LCL filters. *IEEE Transactions on Industry Applications*, 46, 1509–1517. http://dx.doi.org/10.1109/TIA.2010.2049974.

Duesterhoeft, W., Schulz, M. W., & Clarke, E. (1951). Determination of instantaneous currents and voltages by means of alpha, beta, and zero components. *Transactions of the American Institute of Electrical Engineers*, 70, 1248–1255. http://dx.doi.org/10.1109/T-AIEE.1951.5060554.

Ebihara, Y., & Hagiwara, T. (2004). New dilated LMI characterizations for continuous-time multiobjective controller synthesis. *Automatica*, 40, 2003–2009.

Eren, S., Bakhshai, A., & Jain, P. (2012). Control of grid-connected voltage source inverter with lcl filter. In *2012 Twenty-seventh annual IEEE applied power electronics conference and exposition (APEC)* (pp. 1516–1520). http://dx.doi.org/10.1109/APEC.2012.6166021

Francis, B. A., & Wonham, W. M. (1976). The internal model principle of control theory. *Automatica*, 12, 457–465.

Gabe, I., Montagner, V., & Pinheiro, H. (2009). Design and implementation of a robust current controller for VSI connected to the grid through an LCL filter. *IEEE Transactions on Power Electronics*, 24, 1444–1452. http://dx.doi.org/10.1109/TPEL.2009.2016097.

Gahinet, P., Nemirovskii, A., Laub, A. J., & Chilali, M. (1995). *LMI control toolbox user's guide*. Natick, MA: The Math Works Inc.

Geromel, J. C., & Korogui, R. H. (2006). Analysis and synthesis of robust control systems using linear parameter dependent Lyapunov functions. *IEEE Transactions on Automatic Control*, 51, 1984–1989.

IEEE (2011). IEEE:1547 standard for interconnecting distributed resources with electric power systems.

Khajehoddin, S., Karimi-Gharteman, M., Bakhshai, A., & Jain, P. (2014). High quality output current control for single phase grid-connected inverters. In: *2014 twenty-*

ninth annual IEEE applied power electronics conference and exposition (APEC) (pp. 1807–1814). http://dx.doi.org/10.1109/APEC.2014.6803551.

Khajehoddin, S., Karimi-Ghartemani, M., Jain, P., & Bakhshai, A. (2011). A control design approach for three-phase grid-connected renewable energy resources. *IEEE Transactions on Sustainable Energy*, 2, 423–432. http://dx.doi.org/10.1109/TSTE.2011.2158457.

Li, Y.-L., Sun, Y., & Dai, X. (2013). Robust control for an uncertain LCL resonant ICPT system using LMI method. *Control Engineering Practice*, 21, 31–41.

Liserre, M., Teodorescu, R., & Blaabjerg, F. (2006). Stability of photovoltaic and wind turbine grid-connected inverters for a large set of grid impedance values. *IEEE Transactions on Power Electronics*, 21, 263–272. http://dx.doi.org/10.1109/TPEL.2005.861185.

Maccari, L., Do Amaral Santini, C., Pinheiro, H., de Oliveira, R., & Foletto Montagner, V. (2015). Robust optimal current control for grid-connected three-phase pulse-width modulated converters. *IET Power Electronics*, 8, 1490–1499. http://dx.doi.org/10.1049/iet-pel.2014.0787.

Maccari, L. A., Jr., Massing, J. R., Schuch, L., Rech, C., Pinheiro, H., Montagner, V. F., et al. (2012). Robust $\mathcal{H}_\infty$ control for grid connected PWM inverters with LCL filters. In: *Proceedings of the 10th IEEE/IAS international conference on industry applications (INDUSCON 2012)*, Fortaleza, CE, Brazil.

Maccari, L. A., Jr., Massing, J. R., Schuch, L., Rech, C., Pinheiro, H., Oliveira, R. C. L. F. et al. (2014). LMI-based control for grid-connected converters with LCL filters under uncertain parameters. *IEEE Transactions on Power Electronics*, 29, 3376–3785. http://dx.doi.org/10.1109/TPEL.2013.2279015.

Maccari, L. A., Jr., Montagner, V. F., Pinheiro, H., & Oliveira, R. (2012). Robust $\mathcal{H}_2$ control applied to boost converters: Design, experimental validation and performance analysis. *IET Control Theory & Applications*, 6, 1881–1888. http://dx.doi.org/10.1049/iet-cta.2011.0755.

Maccari, Jr., L. A., Santini, C. L. A., Oliveira, R. C. L. F., & Montagner, V. F. (2013). Robust discrete linear quadratic control applied to grid-connected converters with LCL filters. In: *XII Brazilian power electronics conference*, Gramado, Brazil.

Massing, J. R., Stefanello, M., Gründling, H., & Pinheiro, H. (2012). Adaptive current control for grid-connected converters with LCL filter. *IEEE Transactions on Industrial Electronics*, 59, 4681–4693. http://dx.doi.org/10.1109/TIE.2011.2177610.

C.F. Morais, M.F. Braga, R.C.L.F. Oliveira and P.L.D. Peres, Robust state feedback control for discrete-time linear systems via LMIs with a scalar parameter, 2013 American Control Conference, Washington, DC, 2013, pp. 3870-3875. doi: 10.1109/ACC.2013.6580430

Olalla, C., Leyva, R., El Aroudi, A., Garces, P., & Queinnec, I. (2010). LMI robust control design for boost PWM converters. *IET Power Electronics*, 3, 75–85.

Olalla, C., Leyva, R., El Aroudi, A., & Queinnec, I. (2009). Robust LQR control for PWM converters: An LMI approach. *IEEE Transactions on Industrial Electronics*, 56, 2548–2558.

Olalla, C., Queinnec, I., Leyva, R., & Aroudi, A. E. (2011). Robust optimal control of bilinear DC–DC converters. *Control Engineering Practice*, 19, 688–699.

de Oliveira, M. C., Bernussou, J., & Geromel, J. C. (1999). A new discrete-time robust stability condition. *Systems & Control Letters*, 37, 261–265.

de Oliveira, M. C., Geromel, J. C., & Bernussou, J. (2002). Extended $\mathcal{H}_2$ and $\mathcal{H}_\infty$ characterization and controller parametrizations for discrete-time systems. *International Journal of Control*, 75, 666–679.

R.C.L.F. Oliveira, M.C. de Oliveira and P.L.D. Peres, Robust state feedback LMI methods for continuous-time linear systems: Discussions, extensions and numerical comparisons, 2011 IEEE International Symposium on Computer-Aided Control System Design (CACSD), Denver, CO, 2011, pp. 1038-1043. doi: 10.1109/CACSD.2011.6044553

Parker, S., McGrath, B., & Holmes, D. (2014). Regions of active damping control for LCL filters. *IEEE Transactions on Industry Applications*, 50, 424–432. http://dx.doi.org/10.1109/TIA.2013.2266892.

Peaucelle, D., Arzelier, D., Bachelier, O., & Bernussou, J. (2000). A new robust $\mathcal{D}$-stability condition for real convex polytopic uncertainty. *Systems & Control Letters*, 40, 21–30.

Peña-Alzola, R., Liserre, M., Blaabjerg, F., Sebastian, R., Dannehl, J., & Fuchs, F. (2014). Systematic design of the lead-lag network method for active damping in LCL-filter based three phase converters. *IEEE Transactions on Industrial Informatics*, 10, 43–52. http://dx.doi.org/10.1109/TII.2013.2263506.

Pereira, L., Flores, J., Bonan, G., Coutinho, D., & da Silva, J. (2014). Multiple resonant controllers for uninterruptible power supplies – A systematic robust control design approach. *IEEE Transactions on Industrial Electronics*, 61, 1528–1538. http://dx.doi.org/10.1109/TIE.2013.2259781.

Ranganathan, V. T. (1997). Space vector pulsewidth modulation – A status review. *Sadhana*, 22, 675–688. http://dx.doi.org/10.1007/BF02745839.

Ribas, S. P., Maccari, L. A., Jr., Pinheiro, H., Oliveira, R. C., & Montagner, V. F. (2014). Design and implementation of a discrete-time H-infinity controller for uninterruptible power supply systems. *IET Power Electronics*, 7, 2233–2241.

Shaked, U. (2001). Improved LMI representations for the analysis and the design of continuous-time systems with polytopic type uncertainty. *IEEE Transactions on Automatic Control*, 46, 652–656.

de Souza, C. E., Trofino, A., & de Oliveira, J. (2000). Robust $\mathcal{H}_\infty$ control of uncertain linear systems via parameter-dependent Lyapunov functions. In *Proceedings of the 39th IEEE conference on decision and control* (pp. 3194–3199), Sydney, Australia.

Sturm, J. F. (1999). Using SeDuMi 1.02, a MATLAB toolbox for optimization over symmetric cones. *Optimization Methods and Software*, 11–12, 625–653 URL ⟨http://sedumi.mcmaster.ca/⟩.

Sun, L., Li, D., Hu, K., Lee, K. Y., & Pan, F. (2016). On tuning and practical implementation of active disturbance rejection controller: A case study from a regenerative heater in a 1000 mw power plant. *Industrial and Engineering Chemistry Research*, 55, 6686–6695.

Sun, L., Li, D., & Lee, K. Y. (2015). Enhanced decentralized PI control for fluidized bed combustor via advanced disturbance observer. *Control Engineering Practice*, 42, 128–139. http://dx.doi.org/10.1016/j.conengprac.2015.05.014.

Sun, L., Li, D., & Lee, K. Y. (2016). Optimal disturbance rejection for {PI} controller with constraints on relative delay margin. *ISA Transactions*, 63, 103–111. http://dx.doi.org/10.1016/j.isatra.2016.03.014.

Teodorescu, R., Liserre, M., & Rodríguez, P. (2011). *Grid converters for photovoltaic and wind power systems*. Wiley - IEEE. John Wiley & Sons.

Trofino, A., & de Souza, C. E. (2001). Biquadratic stability of uncertain linear systems. *IEEE Transactions on Automatic Control*, 46, 1303–1307.

Umbrí, F., Gordillo, F., Gómez-Estern, F., Salas, F., Portillo, R. C., & Vázquez, S. (2014). Voltage balancing in three-level neutral-point-clamped converters via Luenberger observer. *Control Engineering Practice*, 25, 36–44.

Willis, H., & Scott, W. G. (2000). *Distributed power generation: Planning and evaluation*. *Power Engineering (Willis)*. Taylor & Francis.

Zhang, C., Dragicevic, T., Vasquez, J. C., & Guerrero, J. M. (2014). Resonance damping techniques for grid-connected voltage source converters with lcl filters - A review. In *2014 IEEE international Energy conference (ENERGYCON)* (pp. 169–176) http://dx.doi.org/10.1109/ENERGYCON.2014.6850424.

Zhou, K., Doyle, J. C., & Glover, K. (1996). *Robust and optimal control*. Upper Saddle River, NJ, USA: Prentice Hall.

Zmood, D. N., & Holmes, D. G. (2003). Stationary frame current regulation of PWM inverters with zero steady-state error. *IEEE Transactions on Power Electronics*, 18, 814–822. http://dx.doi.org/10.1109/TPEL.2003.810852.